

Dynamical-decoupling protected nonadiabatic geometric quantum computation with silicon-vacancy centers

M.-R. Yun,¹ L.-L. Yan,^{1,*} Yu Jia,^{2,1,†} S.-L. Su,^{1,‡} and C. X. Shan^{1,§}

¹*School of Physics and Microelectronics, Key Laboratory of Materials Physics of Ministry of Education, Zhengzhou University, Zhengzhou 450052, China*

²*Key Laboratory for Special Functional Materials of Ministry of Education, and School of Materials and Engineering, Henan University, Kaifeng 475001, China*

The negatively charged silicon-vacancy center in diamond has great potential for quantum information processing due to its strong zero-phonon line emission, narrow inhomogeneous broadening, and stable optical transition frequencies. Developing universal quantum computation in silicon-vacancy centers is highly expected. Here, we propose a scheme for nonadiabatic geometric quantum computation in the system, in which silicon-vacancy centers are placed in a one-dimensional phononic waveguide. To improve the performance of the scheme, dynamical decoupling pulse sequences are used to eliminate the impact of the environment on its system. This scheme has the feature of geometric quantum computation that is robust to control errors and has the advantage of dynamical decoupling that is insensitive to environmental impact. Moreover, the feature that qubits are encoded in long-lifetime ground states of silicon-vacancy centers can reduce the decoherence caused by decay. Numerical simulation shows the effectiveness of the silicon-vacancy center system for quantum computation and the improvement of dynamic decoupling pulse in quantum system immunity to environmental noise. Our scheme may provide a promising way toward high-fidelity geometric quantum computation in the solid-state system.

I. INTRODUCTION

Color centers system in diamond has great potential in many applications, such as quantum computation [1–5], state detection [6], coherent manipulation [7], nanoscale sensing [8], and so on. As one of the most widely studied solid defects in diamond, nitrogen-vacancy (NV) center [9, 10] in diamond, due to its bright and stable luminescence properties and long electron spin coherence time, it is widely used in quantum computation [2–5], state detection [6], coherent manipulation [7], nanoscale sensing applications [8]. However, these progresses are localization, and the characteristics of weak and spectral unstable optical transitions hinder the further development of the NV centers [11]. Recently, negatively charged silicon-vacancy (SiV^-) (abbreviated as SiV) center has triggered great attention. The SiV center is formed by replacing two adjacent carbon atoms in the diamond lattice with a silicon atom, and the silicon atom is located between two vacancies. Due to its D_{3d} point group symmetry that can protect it from optical inhomogeneity [12–19]. The SiV center can realize practicable initialization and readout of qubits [20, 21], and the scalability can be achieved by one-dimensional (1D) phononic waveguide [22–24]. In addition, the narrow width (around 5 nm) [25], the zero-phonon line emission [26], and optical coherence properties of SiV centers in diamond lay the foundation for quantum computation [27].

The geometric phase is robust to manipulation errors, so it is often used in quantum computing [28, 29]. The adiabatic Abelian geometric quantum computation (GQC) [30] and adiabatic non-Abelian GQC [31] based on Berry phase [32] and adiabatic non-Abelian phase [33] was first proposed. Nevertheless, adiabatic Abelian GQC and adiabatic non-Abelian GQC need a long evolution time, that is to say, the quantum system will suffer quite a lot of environment-induced decoherence. In order to resolve this problem, nonadiabatic Abelian GQC [34, 35] and nonadiabatic non-Abelian GQC [36, 37] based on nonadiabatic Abelian phase [38] and A-A phase [39] have been proposed. In recent years, various optimization schemes based on NGQC have been proposed, such as optimal control [40–42], the time-optimal technique [43, 44], the shortened path method [45, 46], the noncyclic scheme [47], the reverse engineering scheme [48–51], and so on [52–57]. Some of them are demonstrated in different systems including superconducting circuits [58, 59], trapped ions [60, 61], NV centers in diamond [62, 63] and so on.

On the other hand, the quantum system will inevitably be influenced by its environment, destroying the quantum information therein. A great of schemes have been proposed to protect quantum information processing, including decoherence-free subspace (DFS) [37, 64–70], noiseless subsystems [71–74], and dynamical decoupling (DD) [75–79]. Among these schemes, DD is attractive due to its low resource consumption and excellent results. DD counteracts the interaction between the system and the environment by using some suitable external instantaneous intense pulse sequences, which can effectively improve the immunity of the quantum system to the external environment. These instantaneous intense pulse sequences can be regarded as a generalization of

* llyan@zzu.edu.cn

† jiayu@zzu.edu.cn

‡ slsu@zzu.edu.cn

§ cxshan@zzu.edu.cn

spin-echo experiment [80] that eliminated the effect of unwanted interaction approximately. By choosing appropriate external local control operations, the effect of unwanted interaction can be eliminated approximately. So far, DD has attracted widespread attention in both experiment and theory [81–87]. In other words, DD [76, 88] can average the decoherence caused by the interaction between qubits and its environment to zero, which is an effective tool to protect quantum logic gates [82, 84]. Quantum computation based on geometric phases combined with DD is a promising scheme to realize high-fidelity quantum computation.

Here, we realized NGQC in SiV centers system for the first time, in which SiV centers are placed in a 1D phononic waveguide, where qubits are encoded in long-lifetime ground states of SiV centers. The geometric phase is used to construct a single-qubit quantum gate and a nontrivial two-qubit quantum gate, so our scheme is robust to the control error. Moreover, DD is applied, which uses a series of instantaneous pulses to eliminate the impact of the environment on the system and improve the noise immunity of the quantum system. That is to say, our scheme is immune to both X and Z error as well as the control error.

This paper is organized as follows. In Sec. II, the effective Hamiltonian of SiV centers placed in a 1D phononic waveguide is discussed. The general form of dynamical-decoupling-protected Hamiltonian satisfying nonadiabatic geometric conditions is given in Sec. III. The single-qubit gate and the nontrivial two-qubit gate are constructed in Sec. IV A and Sec. IV B, respectively, and decoupling sequences are added to improve the performance of quantum gates.

II. THE PHYSICAL MODEL

We consider N SiV centers in a 1D phononic waveguide [see Fig. 1 (a)], where the distance between two adjacent SiV centers is fixed, and the atomic structure of the SiV center is shown in Fig. 1 (b).

The structure of negatively charged SiV we consider is determined by the spin-orbit interaction, the Jahn-Teller (JT) effect, and the Zeeman splittings. The Hamiltonian of the SiV center can be written as

$$H_{\text{SiV}} = -\lambda_{\text{SO}} L_z S_z + H_{\text{JT}} + f \gamma_L \vec{B} \cdot \vec{L} + \gamma_s \vec{B} \cdot \vec{S}, \quad (1)$$

where λ_{SO} represents the strength of the spin orbit coupling, γ_L and γ_s are the orbital and spin gyromagnetic ratio, respectively. Suppose the external magnetic field is tilted from the positive direction along the z -axis, so the Zeeman splitting of Hamiltonian can be expressed as $\gamma_s B_z S_z + \gamma_s B_x S_x$. The strength of the JT effect coupling along x (y) can be denoted as Υ_x (Υ_y). And the orbital Zeeman effect is too small to neglect. In the present system, only four ground states and the first excited state are considered. The Hamiltonian of a single SiV center

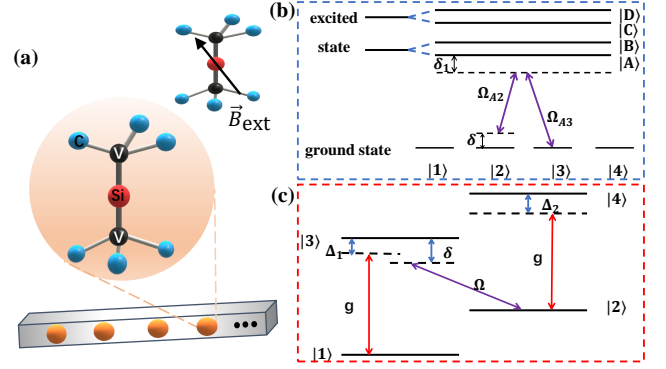


FIG. 1. (a) Illustrative schematic. N SiV centers in a phononic waveguide at fixed positions and the distance between two adjacent SiV centers is fixed. The upper right corner is a diagram of the direction of the external magnetic field. (b) The energy level configuration of the j th SiV center. (c) The effective energy level structure.

can be expressed as

$$H_{\text{SiV}} = \sum_{i=1}^4 \omega_i |i\rangle \langle i| + \omega_a |A\rangle \langle A|, \quad (2)$$

where

$$\begin{aligned} |1\rangle &\equiv |e_-\downarrow\rangle \approx |e_-\downarrow\rangle - \eta_+ |e_-\uparrow\rangle, \\ |2\rangle &\equiv |e_+\uparrow\rangle \approx |e_+\uparrow\rangle - \eta_- |e_-\downarrow\rangle, \\ |3\rangle &\equiv |e_-\downarrow\rangle \approx |e_-\downarrow\rangle + \eta_- |e_+\uparrow\rangle, \\ |4\rangle &\equiv |e_+\uparrow\rangle \approx |e_+\uparrow\rangle + \eta_+ |e_-\downarrow\rangle, \end{aligned}$$

with $\omega_1 \approx -\frac{\Delta+\omega_B}{2} - \frac{\eta_+\omega_x}{2}$, $\omega_2 \approx -\frac{\Delta-\omega_B}{2} - \frac{\eta_-\omega_x}{2}$, $\omega_3 \approx \frac{\Delta-\omega_B}{2} + \frac{\eta_-\omega_x}{2}$, $\omega_4 \approx \frac{\Delta+\omega_B}{2} + \frac{\eta_+\omega_x}{2}$, $\eta_{\pm} = \frac{1}{2} \frac{\omega_x}{\Delta \pm \omega_B}$, $\Delta = \sqrt{\lambda_{\text{SO}}^2 + 4(\Upsilon_x^2 + \Upsilon_y^2)}$, $|A\rangle = |E\downarrow\rangle |E\downarrow\rangle$. The $|e_{\pm}\rangle$ are the eigenstates of the angular momentum operator and the up and down arrow denote the spin-up and spin-down state of the spin projections. In addition, the spin-orbit interaction in the excited state $|E\downarrow\rangle$ is too large to neglect the effect of B_x on the excited state.

We can find that each basis vector in the ground state subspace contains spin-up and spin-down components when the magnetic field and SiV axes are not oriented in the same direction, so the ground state basis vectors can be coupled to all energy levels.

Two lasers coupling $|2\rangle \leftrightarrow |A\rangle$ and $|3\rangle \leftrightarrow |A\rangle$ with Rabi frequencies of Ω_{A2} and Ω_{A3} are used simultaneously, and the frequency are ω_{A2} and ω_{A3} , respectively, as illustrated in Fig. 1 (b). The driving Hamiltonian can be written as

$$H_{\text{d}} = \frac{\Omega_{A2}}{2} |A\rangle \langle 2 | e^{i\omega_{A2}t} + \frac{\Omega_{A3}}{2} |A\rangle \langle 3 | e^{i\omega_{A3}t} + \text{H.c.} \quad (3)$$

The detuning is $\delta_1 = \omega_a - \omega_{A3} - \omega_3 = \omega_a - \omega_{A2} - \delta$.

As for the strain coupling caused by the small displacement of the defect atoms, the interaction in the Born-

Oppenheimer approximation [16, 22, 89] can be approximated as

$$H_s = \sum_{n,j,k} g_{j,k,n} \hat{a}_{j,k} \hat{J}_+^n e^{ikx_n} + \text{H.c.}, \quad (4)$$

where $\hat{J}_- = \hat{J}_+^\dagger = |1\rangle\langle 3| + |2\rangle\langle 4|$ means the lowering operator of the k the mode of the j th branch of the n th SiV center, g is the coupling strength, $a_{j,k}$ ($a_{j,k}^\dagger$) is the annihilation (creation) operator of the k th mode of the j th branch at frequency of $\omega_{j,k}$, and x_n denotes the position of the n th SiV center. So the Hamiltonian of phonon modes can be described by

$$\hat{H}_{ph} = \sum_{j,k} \omega_{j,k} \hat{a}_{j,k}^\dagger \hat{a}_{j,k}. \quad (5)$$

Then, the full Hamiltonian of the system is

$$H_{\text{full}} = H_{\text{SiV}} + H_{\text{ph}} + H_d + H_s \quad (6)$$

In the interaction picture, by considering the rotating-wave approximation and using effective Hamiltonian theory [90, 91] with the condition of $\delta_1, \delta \gg \Omega_{A2}, \Omega_{A3}$, the Hamiltonian of the n th SiV center can be rewritten as

$$H_n(t) = \frac{\Omega}{2} |3\rangle\langle 2| e^{i\delta t} + g a(|3\rangle\langle 1| e^{i\Delta_1 t} + |4\rangle\langle 2| e^{i\Delta_2 t}) + \text{H.c.}, \quad (7)$$

where $\Omega = -\Omega_{A2}^* \Omega_{A3} (2\delta_1 + \delta) / 4\delta_1 (\delta_1 + \delta)$, and the Stark shift can be compensated by lasers [92, 93].

Then, in the condition of $\Delta_1, \Delta_2 \gg g, \Omega$, the effective Hamiltonian can be denoted as

$$H_{\text{neff}} = \frac{\Omega_{\text{eff}}}{2} a^\dagger |1\rangle\langle 2| e^{i(\delta - \Delta_1)t} + \text{H.c.} \quad (8)$$

with $\Omega_{\text{eff}} = \Omega g (\Delta_1 + \delta) / 4\Delta_1 \delta$. We can find that its form is consistent with the Jaynes-Cummings model that can realize quantum computation [94].

III. DYNAMICAL-DECOUPLING-PROTECTED NONADIABATIC GEOMETRIC HAMILTONIAN

In this section, we will use the reverse-engineering scheme to give the target Hamiltonian for the two-level system satisfying nonadiabatic geometric conditions [49]. For the two-level system, the orthogonal auxiliary bases can be chosen as

$$\begin{aligned} |\varphi_1(t)\rangle &= \sin \frac{\theta(t)}{2} e^{-i\phi(t)} |0\rangle - \cos \frac{\theta(t)}{2} |1\rangle, \\ |\varphi_2(t)\rangle &= \cos \frac{\theta(t)}{2} |0\rangle + \sin \frac{\theta(t)}{2} e^{i\phi(t)} |1\rangle, \end{aligned} \quad (9)$$

where the $|0\rangle$ ($|1\rangle$) is the logical qubit, and $\theta(t)$ and $\phi(t)$ are the time-dependent parameters. Then, the Hamilto-

nian of the two-level system can be expressed as

$$\begin{aligned} H(t) &= i \sum_{k \neq l}^2 \langle \varphi_l(t) | \dot{\varphi}_k(t) \rangle | \varphi_l(t) \rangle \langle \varphi_k(t) | \\ &= \Delta(t) (|1\rangle\langle 1| - |0\rangle\langle 0|) + \left[\frac{\Omega(t)}{2} |1\rangle\langle 0| + \text{H.c.} \right]. \end{aligned} \quad (10)$$

Then, we have $\Omega(t) = ie^{i\phi(t)} [\dot{\theta}(t) + i \cos \theta(t) \sin \theta(t) \dot{\phi}(t)]$ and $\Delta(t) = -\frac{1}{2} \sin^2 \theta(t) \dot{\phi}(t)$.

Corresponding to the auxiliary basis vectors, the initial states of the system are

$$\begin{aligned} |\psi_1(0)\rangle &= |\varphi_1(0)\rangle = \sin \frac{\theta(0)}{2} e^{-i\phi(0)} |0\rangle - \cos \frac{\theta(0)}{2} |1\rangle, \\ |\psi_2(0)\rangle &= |\varphi_2(0)\rangle = \cos \frac{\theta(0)}{2} |0\rangle + \sin \frac{\theta(0)}{2} e^{i\phi(0)} |1\rangle. \end{aligned} \quad (11)$$

After a cyclic evolution, the evolution operator $U(T) = e^{-i\gamma(T)} |\psi_1(0)\rangle\langle\psi_1(0)| + e^{i\gamma(T)} |\psi_2(0)\rangle\langle\psi_2(0)|$ can be written as

$$\begin{aligned} &\begin{pmatrix} \cos \gamma(T) + i \cos \theta_0 \sin \gamma(T) & ie^{-i\phi_0} \sin \gamma(T) \sin \theta_0 \\ ie^{i\phi_0} \sin \gamma(T) \sin \theta_0 & \cos \gamma(T) - i \cos \theta_0 \sin \gamma(T) \end{pmatrix} \\ &= e^{-i\gamma(T)\mathbf{n}\cdot\boldsymbol{\sigma}}, \end{aligned} \quad (12)$$

where $\theta_0 \equiv \theta(0)$, $\phi_0 \equiv \phi(0)$, $\gamma(T) = i \int_0^T \langle \varphi_1(t) | \dot{\varphi}_1(t) \rangle dt = -i \int_0^T \langle \varphi_2(t) | \dot{\varphi}_2(t) \rangle dt = \frac{1}{2} \int_0^T [1 - \cos \theta(t) \dot{\phi}(t)] dt = \frac{1}{2} \oint_C [1 - \cos \theta(t)] d\phi$, it can be clearly seen that the $\gamma(T)$ is half of the solid angle, independent of the evolution details, and $\mathbf{n} = [\sin \theta(0) \cos \phi(0), \sin \theta(0) \sin \phi(0), \cos \theta(0)]$, $\boldsymbol{\sigma} = (\sigma_x, \sigma_y, \sigma_z)$. The schematic diagram of the evolution path is shown in Fig. 2(a). General single-qubit gates can be constructed by selecting different parameters. Universal quantum computation can be realized by a non-trivial two-qubit quantum gate assist with an arbitrary single-qubit gate [95].

For the two-qubit gate, the auxiliary bases can be chosen as

$$\begin{aligned} |\varphi_1(t)\rangle &= |00\rangle, \\ |\varphi_2(t)\rangle &= \cos \frac{\theta(t)}{2} |01\rangle + \sin \frac{\theta(t)}{2} e^{i\phi(t)} |10\rangle, \\ |\varphi_3(t)\rangle &= \sin \frac{\theta(t)}{2} e^{-i\phi(t)} |01\rangle - \cos \frac{\theta(t)}{2} |10\rangle, \\ |\varphi_4(t)\rangle &= |11\rangle. \end{aligned} \quad (13)$$

The general form of Hamiltonian of the two-qubit gate is

$$\begin{aligned} H_{\text{two}}(t) &= i \sum_{k \neq l}^4 \langle \varphi_l(t) | \dot{\varphi}_k(t) \rangle | \varphi_l(t) \rangle \langle \varphi_k(t) | \\ &= \frac{\Omega_{\text{two}}(t)}{2} |01\rangle\langle 10| + \text{H.c..} \end{aligned} \quad (14)$$

The evolution operator of this system U_2 can be expressed as

$$\begin{aligned}
U_2(T) &= |\varphi_1(T)\rangle\langle\varphi_1(0)| + e^{-i\gamma(T)}|\varphi_2(0)\rangle\langle\varphi_2(0)| + e^{i\gamma(T)}|\varphi_3(0)\rangle\langle\varphi_3(0)| + \varphi_4(T)\rangle\langle\varphi_4(0)| \\
&= \begin{pmatrix} 1 & 0 & 0 & 0 \\ 0 & \cos\gamma(T) - i\cos\theta(0)\sin\gamma(T) & -ie^{-i\varphi(0)}\sin\theta(0)\sin\gamma(T) & 0 \\ 0 & -ie^{i\varphi(0)}\sin\theta(0)\sin\gamma(T) & \cos\gamma(T) + i\cos\theta(0)\sin\gamma(T) & 0 \\ 0 & 0 & 0 & 1 \end{pmatrix}.
\end{aligned} \tag{15}$$

By selecting appropriate parameters, we can build a nontrivial two-qubit quantum geometric gate. The general geometric quantum computation can be achieved by combining universal single-qubit gates.

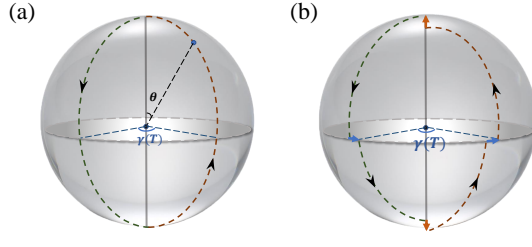


FIG. 2. The evolution paths for the single-loop NGQC scheme (a) without and (b) with impact of the environment and decoupled pulses (take the basic pulse as an example).

In the process of gate implementation, evolution inevitably receives the influence of the surrounding environment, which can lead to a reduction in fidelity. Next, a set of general pulse sequences that can cancel the system and environment are derived.

Here we consider the system and environment coupling Hamiltonian [75, 77, 78]

$$H_{\text{se}} = H_s \otimes H_e = \sum_{\alpha=x,y,z} \sigma^\alpha \otimes B^\alpha, \tag{16}$$

where σ^α denotes the system Hamiltonian and B^α expresses the environment operator. The system evolution operator expressed as $f_\tau = e^{-i\tau H_{\text{se}}}$, we assume these pulses last for a period of time \mathcal{D} with strength λ , and $\mathcal{D}\lambda = \frac{\pi}{2}$, in the ideal case, $\mathcal{D} \rightarrow 0$, $\lambda \rightarrow \infty$. Now, we apply two X-pulse $X = e^{i\mathcal{D}\lambda\sigma^x} \otimes I_B = e^{-i\frac{\pi}{2}\sigma^x} \otimes I_B = -i\sigma^x \otimes I_B$ on the system, we have

$$\sigma^x H_{\text{se}} \sigma^x = \sigma^x \otimes B^x - \sigma^y \otimes B^y - \sigma^z \otimes B^z, \tag{17}$$

which means that $X f_\tau X f_\tau$ pulse sequence can cancel both the y and z contributions. Evolution can be described as

$$X f'_{2\tau} = X f_\tau X f_\tau = e^{-2i\tau(\sigma^x \otimes B^x + H_e)} + \mathcal{O}(\tau^2). \tag{18}$$

Then we apply Y-pulse $Y = e^{i\mathcal{D}\lambda\sigma^y} \otimes I_B = e^{-i\frac{\pi}{2}\sigma^y} \otimes I_B = -i\sigma^y \otimes I_B$ on the system,

$$\begin{aligned}
Y f'_{2\tau} Y f'_{2\tau} &= Y X f_\tau X f_\tau Y X f_\tau X f_\tau \\
&= Z f_\tau X f_\tau Z f_\tau X f_\tau \\
&= e^{-i4\tau H_e} + \mathcal{O}(\tau^2),
\end{aligned} \tag{19}$$

so when evolution time $t = 4\tau$, the system can decouple from the environment, i.e., $Z X Z X$ are universal decoupling pulse sequences that can reduce the impact of the environment on the system. Here, we can repeat the basic DD sequence periodically named periodic dynamical decoupling [81] to further enhance the performance of the system, the basic pulse sequence (four-beam pulse), the pulse sequence with a period of two (eight-beam pulse), and the pulse sequence with a period of three (twelve-beam pulse) are shown in Fig. 3 (a), (b), and (c), respectively.

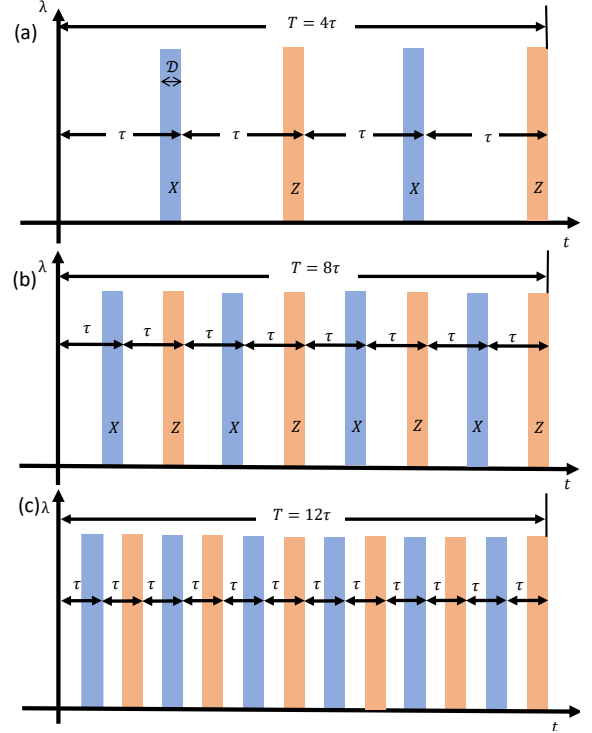


FIG. 3. Schematic diagram of period decoupled pulses. (a) The base four-beam pulse. (b) The eight-beam pulse with period two. (c) The twelve-beam pulse with period three.

Then, the decoherence caused by the interaction between the quantum system and the environment can be inhibited greatly. The schematic diagram of the evolution with the impact of the environment and decoupled pulses is shown in Fig. 2(b). Because of the interaction of the environment, the trajectory of the evolution state will have a slight deviation from the ideal situation, i.e., the evolution shown in Fig. 2(a). This

deviation can be eliminated by the dynamic decoupling pulses (represented by orange and blue arrows with solid lines), so as to achieve the ideal evolution. Therefore, the dynamical-decoupling-protected nonadiabatic geometric quantum computation can be realized in the SiV centers by constructing the Hamiltonian in the form of Eq. (10) and Eq. (14) and adding the dynamic decoupling pulses.

IV. IMPLEMENTATION

By combining a set of universal single-qubit gates and a nontrivial two-qubit gate, universal quantum can be realized, in this section, we will show how to use SiV centers to realize general geometric quantum logic gates.

A. The single-qubit gate

Based on the effective Hamiltonian of the SiV center system Eq. 8, we construct a single-qubit quantum gate, with only one SiV center placed on the 1D phononic waveguide, i.e. $n = 1$. For simplicity, we consider the single excitation mode, regard $|11\rangle$ and $|20\rangle$ as logical qubits $|0\rangle_L$ and $|1\rangle_L$, where $|11\rangle$ ($|20\rangle$) is the abbreviation $|1\rangle \otimes |1\rangle$ ($|2\rangle \otimes |0\rangle$) and the first qubit means the energy level of SiV center, the second qubit means the Fork state of phonon. In this case, the Hamiltonian of the single qubit is in the same form as Eq. (10). The degree of conformity between the Hamiltonian in Eq. (6) and Eq. (8) is shown in Fig. 4, in which the red (blue) dotted line represents the evolution of the population of $|0\rangle_L$ ($|1\rangle_L$) in Eq. (6), and the red (blue) solid line indicates the evolution of the population of $|0\rangle_L$ ($|1\rangle_L$) in Eq. (8). It can be seen that the effective Hamiltonian and the original Hamiltonian agree very well.

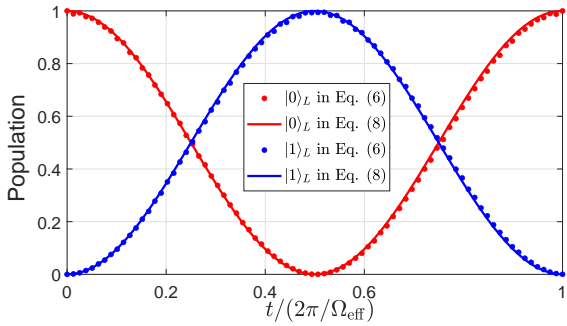


FIG. 4. The comparison of the population of $|0\rangle_L$ and $|1\rangle_L$ from Eq. (6) with the Eq. (8), where $\Omega/2\pi = 10\text{MHz}$, $g/2\pi = 5\text{MHz}$, $\Delta_1/2\pi = 100\text{MHz}$, $\Delta_2/2\pi = 500\text{MHz}$, $\delta = \Delta_1$. The red (black) points and solid lines represent the population of $|0\rangle_L$ ($|1\rangle_L$) evolved under the full and effective Hamiltonian, respectively.

We take a single qubit phase gate and a SWAP gate as examples. For the phase gate, the polar angle ($\theta(t)$) and the azimuth angle ($\phi(t)$) starting from the north pole

($\theta(0) = 0, \phi(0)$), passing through the south pole, a phase sudden change occurs ($\theta(t) = \pi, \phi(t) = \phi(0) + \pi/4$), and then returning to the north pole. The Hamiltonian can be expressed as

$$\begin{cases} \frac{\dot{\theta}(t)}{2}[-\sin\phi(0)\sigma_x + \cos\phi(0)\sigma_y], & t \in [0, \frac{T}{2}], \\ \frac{\dot{\theta}(t)}{2}[-\sin(\phi(0) + \frac{\pi}{4})\sigma_x + \cos(\phi(0) + \frac{\pi}{4})\sigma_y], & t \in (\frac{T}{2}, T], \end{cases} \quad (20)$$

and the parameters meet $\int_0^{T/2} \dot{\theta}(t)dt = \pi/2$, $\int_{T/2}^T \dot{\theta}(t)dt = -\pi/2$.

For the SWAP gate (ignore the global phase), the polar angle and the azimuth angle starting from ($\theta(0) = \frac{\pi}{2}, \phi(0) = 0$), passing the south pole and the north pole and back to the starting point. The parameters in the Hamiltonian quantity satisfy

$$\begin{cases} \int_0^{T_1} \dot{\theta}(t)dt = \theta(0), & \phi(t) = 0, \quad t \in [0, T_1], \\ \int_{T_1}^{T_2} \dot{\theta}(t)dt = \pi, & \phi(t) = -\frac{\pi}{2}, \quad t \in (T_1, T_2], \\ \int_{T_2}^T \dot{\theta}(t)dt = \pi - \theta(0), & \phi(t) = 0, \quad t \in (T_2, T]. \end{cases} \quad (21)$$

Then, add the decoupling sequence in Fig. 3 to Hamiltonian to further improve the performance of the gate. We use the fidelity defined as

$$F = \langle \psi_{\text{ideal}} | \rho(T) | \psi(T) \rangle \quad (22)$$

to evaluate the performance of the gate, where $|\psi_{\text{ideal}}\rangle = U(T)|\psi(0)\rangle$ is the ideal final state, the $\psi(T)$ is the actual final state, and the $\rho(T)$ is the density matrix.

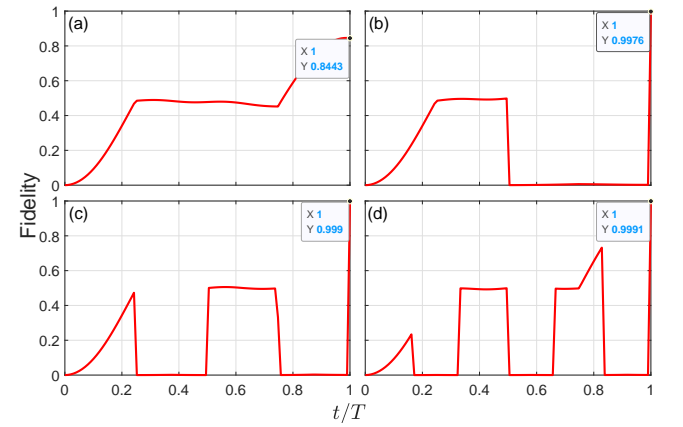


FIG. 5. The fidelity of the SWAP gate driven by Eq. (20). (a) The fidelity without being protected by dynamical decoupling. (b) The fidelity with being protected by four decoupled pulse sequences dynamical decoupling. (c) The fidelity with being protected by eight decoupled pulse sequences dynamical decoupling. (d) The fidelity with being protected by twelve decoupled pulse sequences dynamical decoupling. The control parameters are set the same as Fig. 4.

According to Ref. [96], the Liouville equation $\dot{\rho}(t) = -i[H_{\text{sum}}(t), \rho(t)]$ can be used to calculate the density matrix, where $H_{\text{sum}}(t) = H(t) + H_E(t) + H_I(t)$ is the total

Hamiltonian, $H_E(t)$ is the Hamiltonian of the environment, and the $H_I(t)$ is the Hamiltonian of the interaction between the system and the environment. In the numerical simulations, we use the single-qubit SWAP (phase) gate $U(T) = \exp(-i\pi\sigma_x/2)$ ($U(T) = \exp(-i\pi\sigma_z/2)$), $\psi(0) = |0\rangle_L$, and the environment Hamiltonian $H_E(t) = G_1[I_{\text{sys}} \otimes \sum_{k=x,y,z} \sigma_k]$ with I_{sys} means the identity matrix of the system, the $H_I(t) = G_2[H(t) \otimes \sum_{k=x,y,z} \sigma_k]$, where $\Omega_{\text{eff}}/G_1 = \Omega_{\text{eff}}/G_2 = 3 \times 10^3$. From Fig. 5 (Fig. 6), we can see the fidelity of the SWAP (phase) gate is significantly improved, when the decoupling pulse sequences are four, eight, and twelve, the fidelity can reach 0.9976 (0.9974), 0.999 (0.9989), and 0.9991 (0.9991), respectively.

We further demonstrate the robustness of our scheme against the decoherence and dephasing coefficients impacted by environment (G_1 and G_2), which adjust the value of coefficients in numerical simulation. The fidelity of the SWAP gate (phase gate) changing with the strength of the environmental interaction is shown in Fig. 7(a)((b)), where the black line represents the fidelity not protected by dynamic decoupling pulse, and the red line represents the fidelity protected by a group of the basic dynamic decoupling pulse (four decoupling pulses). From this, we can see that the dynamical decoupling pulse greatly protects the nonadiabatic geometric quantum gates from environment-induced decoherence and decay.

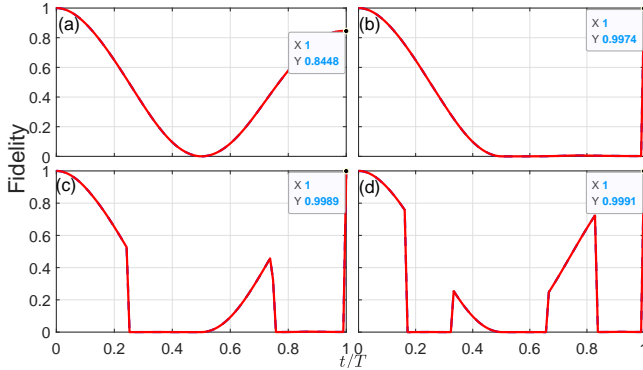


FIG. 6. The fidelity of the phase gate driven by Eq. (20). (a) The fidelity without being protected by dynamical decoupling. (b) The fidelity with being protected by four decoupled pulse sequences dynamical decoupling. (c) The fidelity with being protected by eight decoupled pulse sequences dynamical decoupling. (d) The fidelity with being protected by twelve decoupled pulse sequences dynamical decoupling. The control parameters are set the same as Fig. 4.

B. The two-qubit quantum gate

Here, we consider two SiV centers in the phononic waveguide, we define the effective detuning $\delta - \Delta_1 = \Lambda_1$,

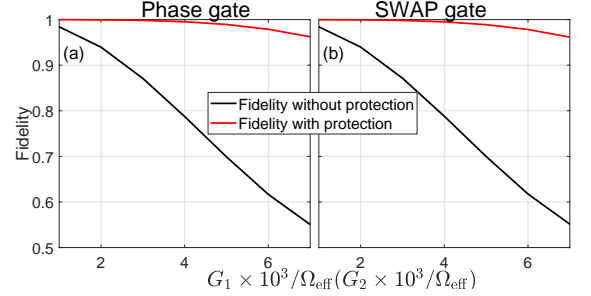


FIG. 7. The fidelity of the phase gate (a) and the SWAP gate (b) varying with the strength of environmental interaction. The control parameters are set the same as Fig. 4.

and the Hamiltonian

$$H_n = \frac{\Omega_{\text{eff}}}{2} a^\dagger |1\rangle \langle 2| e^{i\Lambda_n t} \quad (23)$$

of the n th SiV center when $\Lambda_n \gg \Omega_{\text{eff}}$, the effective Hamiltonian of the system can be written as

$$H_{\text{two}} = -\Omega_{\text{eff}}^2 \frac{\Lambda_1 + \Lambda_2}{8\Lambda_1\Lambda_2} \sigma_1^- \sigma_2^+ e^{i(\Lambda_1 - \Lambda_2)t} + \text{H.c.}, \quad (24)$$

where σ_1^- denotes the energy level decline of the first SiV center, σ_2^+ means the energy level rise of the second SiV center. Now, similar to the single qubit gate, we code $|1\rangle_{\text{SiV}}$ ($|2\rangle_{\text{SiV}}$) as logical qubit $|0\rangle_L$ ($|1\rangle_L$), so the Hamiltonian in Eq. (24) can be written in the following form in the basic $|00\rangle_L |01\rangle_L |10\rangle_L |11\rangle_L$,

$$H_2 = - \begin{pmatrix} 0 & 0 & 0 & 0 \\ 0 & \Lambda_2 - \Lambda_1 & \frac{\Omega_{\text{eff}}^2(\Lambda_1 + \Lambda_2)}{8\Lambda_1\Lambda_2} & 0 \\ 0 & \frac{\Omega_{\text{eff}}^2(\Lambda_1 + \Lambda_2)}{8\Lambda_1\Lambda_2} & \Lambda_1 - \Lambda_2 & 0 \\ 0 & 0 & 0 & 0 \end{pmatrix}. \quad (25)$$

The reduced Hamiltonian of $|01\rangle_L$ and $|10\rangle_L$ is in the same form as Eq. (14), and it can be seen from Fig. 8 that the original Hamiltonian and the effective Hamiltonian are highly consistent.

Here, we choose $\Lambda_1 = \Lambda_2$, and $\gamma(T) = \pi/2$, $\theta(0) = \pi/2$, and $\varphi(0) = \pi$, the iSWAP gate can be achieved. The parameters in Hamiltonian meet

$$\begin{cases} \int_0^{T_1} O_{\text{eff}} dt = \theta(0), & \phi(t) = \pi, \quad t \in [0, T_1], \\ \int_{T_1}^{T_2} O_{\text{eff}} dt = \pi, & \phi(t) = \pi + \frac{\pi}{2}, \quad t \in (T_1, T_2], \\ \int_{T_2}^T O_{\text{eff}} dt = \pi - \theta(0), & \phi(t) = \pi, \quad t \in (T_2, T]. \end{cases} \quad (26)$$

The azimuth angle ϕ changes twice at the south pole and north pole.

The system Hamiltonian is $H_2(t)$ in Eq. (7), and the environment Hamiltonian and interaction Hamiltonian is $H_E(t) = G_1[I_{\text{sys}} \otimes \sum_{k=x,y,z} \sigma_k]$ and $H_I(t) = G_2[H_2(t) \otimes \sum_{k=x,y,z} \sigma_k]$, the parameters setting are the same as Sec. IV A. The initial state is set as $|01\rangle_L$, the

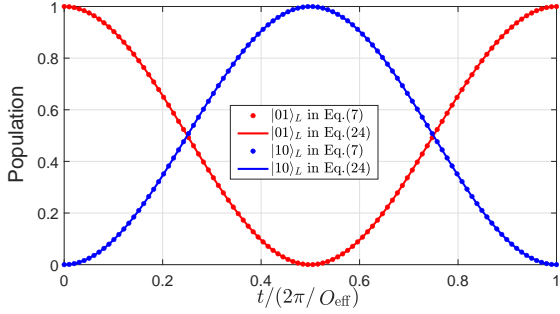


FIG. 8. The comparison of the population of $|01\rangle_L$ and $|10\rangle_L$ from Eq. (7) with the Eq. (24), where $\Omega/2\pi = 10$ MHz, $g/2\pi = 5$ MHz, $\Delta_1/2\pi = 80$ MHz, $\Delta_2/2\pi = 150$ MHz, $\delta = 20$ MHz. The red (black) points and solid lines represent the population of $|01\rangle_L$ ($|10\rangle_L$) evolved under the full and effective Hamiltonian, respectively, where $O_{\text{eff}} = \Omega_{\text{eff}}^2 \frac{\Delta_1 + \Delta_2}{4\Delta_1 \Delta_2}$.

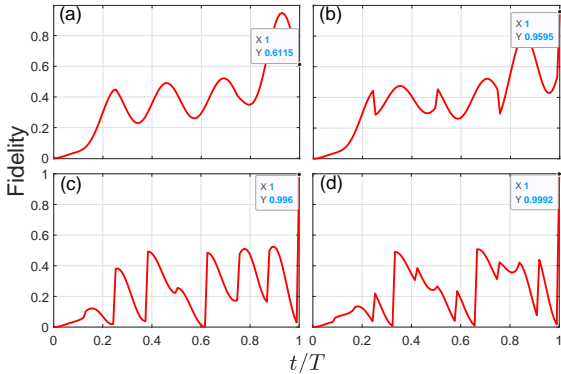


FIG. 9. The fidelity of the gate driven by Eq. (26). (a) The fidelity without being protected by dynamical decoupling. (b) The fidelity with being protected by four decoupled pulse sequences dynamical decoupling. (c) The fidelity with being protected by eight decoupled pulse sequences dynamical decoupling. (d) The fidelity with being protected by twelve decoupled pulse sequences dynamical decoupling. The control parameters are set the same as Fig. 8.

fidelity F defined as Eq. (22) is shown as Fig. 9. Due to environmental impaction, the decoherence and dephasing coefficients (G_1 and G_2) compared with the effective Rabi frequency O_{eff} of the model are too large to maintain high fidelity, as shown in Fig. 9(a). So, add the decoupling sequence in Fig. 3 to Hamiltonian to further improve the performance of the gate. When the decoupling pulse sequences are four, eight, and twelve, the fidelity can reach 0.9595, 0.996, and 0.9992 respectively, as shown in Fig. 9(b), (c), and (d). From the result of numerical simulations, the dynamical decoupling can protect the quantum system against the decoherence and dephasing coming from the environment. The fidelity of the iSWAP gate varying with the strength of environmental interaction G_1 and G_2 is shown in Fig. 10 in which the black line with square marks represents the

fidelity without dynamical decoupling sequences, and the red line with circle marks means fidelity protected by a set of basic dynamical decoupling sequence, i.e. the pulse sequences shown in Fig. 3(a), we can see the fidelity can be protected greatly.

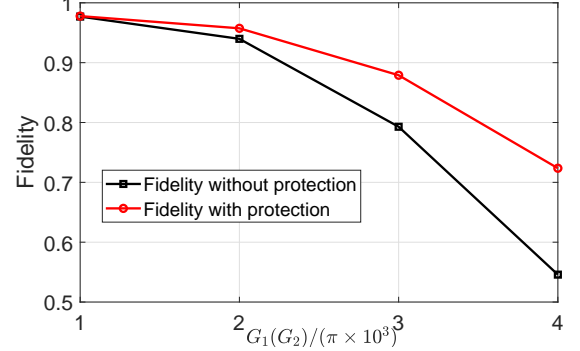


FIG. 10. The fidelity of the iSWAP gate varies with the strength of environmental interaction G_1 and G_2 . The control parameters are set the same as Fig. 9.

V. CONCLUSION

We use the SiV centers to realize universal NGQC for the first time, and the dynamical decoupling pulse sequences are used to improve the immunity of the quantum system to environmental impaction. The scalability can be achieved by a 1D phononic waveguide. Besides the scalability, our scheme is easy to initialize and read out. In summary, our scheme can protect quantum gates from both the control error caused by actual operation due to the intrinsic robustness of geometric quantum logic gates and the dephasing caused by the environment, which are two obstacles to the realization of high-fidelity quantum logic gates. In addition, logical qubits are encoded in long-lifetime ground states of SiV centers, which can reduce the decoherence caused by spontaneous emission. Numerical simulations show the superiority of our scheme in preparing quantum logic gates. Therefore, our scheme may be promising for implementing high-fidelity geometric quantum computation in the solid-state system.

VI. ACKNOWLEDGEMENT

This work was supported by the National Natural Science Foundation of China under Grants (No. 12274376, No. U21A20434, No. 12074346), and a major science and technology project of Henan Province under Grant No. 221100210400, and the Natural Science Foundation of Henan Province under Grant No. 232300421075 and 212300410085.

[1] Sébastien Pezzagna and Jan Meijer, “Quantum computer based on color centers in diamond,” *Applied Physics Reviews* **8**, 011308 (2021), <https://doi.org/10.1063/5.0007444>.

[2] Meng-Ru Yun, Fu-Qiang Guo, L.-L. Yan, Erjun Liang, Y. Zhang, S.-L. Su, C. X. Shan, and Yu Jia, “Parallel-path implementation of nonadiabatic geometric quantum gates in a decoherence-free subspace with nitrogen-vacancy centers,” *Phys. Rev. A* **105**, 012611 (2022).

[3] Zhao Jin, S. L. Su, and Shou Zhang, “Preparation of a steady entangled state of two nitrogen-vacancy centers by simultaneously utilizing two dissipative factors,” *Phys. Rev. A* **100**, 052332 (2019).

[4] Jian Zhou, Wei-Can Yu, Yu-Mei Gao, and Zheng-Yuan Xue, “Cavity qed implementation of non-adiabatic holonomies for universal quantum gates in decoherence-free subspaces with nitrogen-vacancy centers,” *Opt. Express* **23**, 14027–14035 (2015).

[5] Peng-Bo Li, Shao-Yan Gao, Hong-Rong Li, Sheng-Li Ma, and Fu-Li Li, “Dissipative preparation of entangled states between two spatially separated nitrogen-vacancy centers,” *Phys. Rev. A* **85**, 042306 (2012).

[6] F. Jelezko, T. Gaebel, I. Popa, A. Gruber, and J. Wrachtrup, “Observation of coherent oscillations in a single electron spin,” *Phys. Rev. Lett.* **92**, 076401 (2004).

[7] Bo Li, Peng-Bo Li, Yuan Zhou, Sheng-Li Ma, and Fu-Li Li, “Quantum microwave-optical interface with nitrogen-vacancy centers in diamond,” *Phys. Rev. A* **96**, 032342 (2017).

[8] L. Rondin, J-P. Tetienne, T. Hingant, J-F. Roch, P. Maletinsky, and V. Jacques, “Magnetometry with nitrogen-vacancy defects in diamond,” *Reports on Progress in Physics* **77**, 056503 (2014).

[9] Marcus W. Doherty, Neil B. Manson, Paul Delaney, Fedor Jelezko, Jörg Wrachtrup, and Lloyd C.L. Hollenberg, “The nitrogen-vacancy colour centre in diamond,” *Physics Reports* **528**, 1–45 (2013), the nitrogen-vacancy colour centre in diamond.

[10] Lilian Childress, Ronald Walsworth, and Mikhail Lukin, “Atom-like crystal defects: From quantum computers to biological sensors,” *Physics Today* **67**, 38–43 (2014).

[11] H. Bernien, B. Hensen, W. Pfaff, G. Koolstra, M. S. Blok, L. Robledo, T. H. Taminiau, M. Markham, D. J. Twitchen, L. Childress, and R. Hanson, “Heralded entanglement between solid-state qubits separated by three metres,” *Nature* **497**, 86–90 (2013).

[12] A. Sipahigil, R. E. Evans, D. D. Sukachev, M. J. Burek, J. Borregaard, M. K. Bhaskar, C. T. Nguyen, J. L. Pacheco, H. A. Atikian, C. Meuwly, R. M. Camacho, F. Jelezko, E. Bielejec, H. Park, M. Lončar, and M. D. Lukin, “An integrated diamond nanophotonics platform for quantum-optical networks,” *Science* **354**, 847–850 (2016).

[13] Andreas Dietrich, Kay D. Jahnke, Jan M. Binder, Tokuyuki Teraji, Junichi Isoya, Lachlan J. Rogers, and Fedor Jelezko, “Isotopically varying spectral features of silicon-vacancy in diamond,” *New Journal of Physics* **16**, 113019 (2014).

[14] Jonas Nils Becker and Christoph Becher, “Coherence properties and quantum control of silicon vacancy color centers in diamond,” *physica status solidi (a)* **214**, 1700586 (2017).

[15] Elisa Londero, Gergő Thiering, Lukas Razinkovas, Adam Gali, and Audrius Alkauskas, “Vibrational modes of negatively charged silicon-vacancy centers in diamond from ab initio calculations,” *Phys. Rev. B* **98**, 035306 (2018).

[16] Srujan Meesala, Young-Ik Sohn, Benjamin Pingault, Linbo Shao, Haig A. Atikian, Jeffrey Holzgrafe, Mustafa Gündoğan, Camille Stavrakas, Alp Sipahigil, Cleaven Chia, Ruffin Evans, Michael J. Burek, Mian Zhang, Lue Wu, Jose L. Pacheco, John Abraham, Edward Bielejec, Mikhail D. Lukin, Mete Atatüre, and Marko Lončar, “Strain engineering of the silicon-vacancy center in diamond,” *Phys. Rev. B* **97**, 205444 (2018).

[17] Péter Udvarhelyi, Roland Nagy, Florian Kaiser, Sang-Yun Lee, Jörg Wrachtrup, and Adam Gali, “Spectrally stable defect qubits with no inversion symmetry for robust spin-to-photon interface,” *Phys. Rev. Applied* **11**, 044022 (2019).

[18] Matthew W. Day, Kelsey M. Bates, Christopher L. Smallwood, Rachel C. Owen, Tim Schröder, Edward Bielejec, Ronald Ulbricht, and Steven T. Cundiff, “Coherent interactions between silicon-vacancy centers in diamond,” *Phys. Rev. Lett.* **128**, 203603 (2022).

[19] Christian Hepp, Tina Müller, Victor Waselowski, Jonas N. Becker, Benjamin Pingault, Hadwig Sternschulte, Doris Steinmüller-Nethl, Adam Gali, Jerônimo R. Maze, Mete Atatüre, and Christoph Becher, “Electronic structure of the silicon vacancy color center in diamond,” *Phys. Rev. Lett.* **112**, 036405 (2014).

[20] Lachlan J. Rogers, Kay D. Jahnke, Mathias H. Metsch, Alp Sipahigil, Jan M. Binder, Tokuyuki Teraji, Hitoshi Sumiya, Junichi Isoya, Mikhail D. Lukin, Philip Hemmer, and Fedor Jelezko, “All-optical initialization, readout, and coherent preparation of single silicon-vacancy spins in diamond,” *Phys. Rev. Lett.* **113**, 263602 (2014).

[21] Benjamin Pingault, David-Dominik Jarausch, Christian Hepp, Lina Klintberg, Jonas N. Becker, Matthew Markham, Christoph Becher, and Mete Atatüre, “Coherent control of the silicon-vacancy spin in diamond,” *Nature Communications* **8**, 15579 (2017).

[22] M.-A. Lemonde, S. Meesala, A. Sipahigil, M. J. A. Schuetz, M. D. Lukin, M. Loncar, and P. Rabl, “Phonon networks with silicon-vacancy centers in diamond waveguides,” *Phys. Rev. Lett.* **120**, 213603 (2018).

[23] Yi-Fan Qiao, Jia-Qiang Chen, Xing-Liang Dong, Bo-Long Wang, Xin-Lei Hei, Cai-Peng Shen, Yuan Zhou, and Peng-Bo Li, “Generation of greenberger-horne-zeilinger states for silicon-vacancy centers using a decoherence-free subspace,” *Phys. Rev. A* **105**, 032415 (2022).

[24] Xinke Li, Shengli Ma, Jikun Xie, Yalong Ren, and Fuli Li, “Dissipative generation of steady-state entanglement of two separated siv– centers coupled to photonic crystal cavities,” *Quantum Information Processing* **19**, 301 (2020).

[25] Gergő Thiering and Adam Gali, “Ab initio magneto-optical spectrum of group-iv vacancy color centers in diamond,” *Phys. Rev. X* **8**, 021063 (2018).

[26] Stefan Häußler, Gergő Thiering, Andreas Dietrich, Niklas Waasem, Tokuyuki Teraji, Junichi Isoya, Takayuki Iwasaki, Mutsuko Hatano, Fedor Jelezko, Adam Gali,

and Alexander Kubanek, "Photoluminescence excitation spectroscopy of siv— and gev— color center in diamond," *New Journal of Physics* **19**, 063036 (2017).

[27] T. D. Ladd, F. Jelezko, R. Laflamme, Y. Nakamura, C. Monroe, and J. L. O'Brien, "Quantum computers," *Nature* **464**, 45–53 (2010).

[28] Paolo Solinas, Paolo Zanardi, and Nino Zanghì, "Robustness of non-abelian holonomic quantum gates against parametric noise," *Phys. Rev. A* **70**, 042316 (2004).

[29] Shi-Liang Zhu and Paolo Zanardi, "Geometric quantum gates that are robust against stochastic control errors," *Phys. Rev. A* **72**, 020301 (2005).

[30] Jonathan A. Jones, Vlatko Vedral, Artur Ekert, and Giuseppe Castagnoli, "Geometric quantum computation using nuclear magnetic resonance," *Nature* **403**, 869–871 (2000).

[31] Paolo Zanardi and Mario Rasetti, "Holonomic quantum computation," *Physics Letters A* **264**, 94–99 (1999).

[32] Michael Victor Berry, "Quantal phase factors accompanying adiabatic changes," *Proceedings of the Royal Society of London. A. Mathematical and Physical Sciences* **392**, 45–57 (1984).

[33] Frank Wilczek and A. Zee, "Appearance of gauge structure in simple dynamical systems," *Phys. Rev. Lett.* **52**, 2111–2114 (1984).

[34] Wang Xiang-Bin and Matsumoto Keiji, "Nonadiabatic conditional geometric phase shift with nmr," *Phys. Rev. Lett.* **87**, 097901 (2001).

[35] Shi-Liang Zhu and Z. D. Wang, "Implementation of universal quantum gates based on nonadiabatic geometric phases," *Phys. Rev. Lett.* **89**, 097902 (2002).

[36] Erik Sjöqvist, D M Tong, L Mauritz Andersson, Björn Hessmo, Markus Johansson, and Kuldip Singh, "Non-adiabatic holonomic quantum computation," *New Journal of Physics* **14**, 103035 (2012).

[37] G. F. Xu, J. Zhang, D. M. Tong, Erik Sjöqvist, and L. C. Kwek, "Nonadiabatic holonomic quantum computation in decoherence-free subspaces," *Phys. Rev. Lett.* **109**, 170501 (2012).

[38] J. Anandan, "Non-adiabatic non-abelian geometric phase," *Physics Letters A* **133**, 171–175 (1988).

[39] Y. Aharonov and J. Anandan, "Phase change during a cyclic quantum evolution," *Phys. Rev. Lett.* **58**, 1593–1596 (1987).

[40] Chen-Yue Guo, L.-L. Yan, Shou Zhang, Shi-Lei Su, and Weibin Li, "Optimized geometric quantum computation with a mesoscopic ensemble of rydberg atoms," *Phys. Rev. A* **102**, 042607 (2020).

[41] Mengru Yun, Fu-Qiang Guo, Meng Li, L.-L. Yan, M. Feng, Y.-X. Li, and S.-L. Su, "Distributed geometric quantum computation based on the optimized-control-technique in a cavity-atom system via exchanging virtual photons," *Opt. Express* **29**, 8737–8750 (2021).

[42] Meng Li, F.-Q. Guo, Z. Jin, L.-L. Yan, E.-J. Liang, and S.-L. Su, "Multiple-qubit controlled unitary quantum gate for rydberg atoms using shortcut to adiabaticity and optimized geometric quantum operations," *Phys. Rev. A* **103**, 062607 (2021).

[43] Tao Chen and Zheng-Yuan Xue, "Nonadiabatic geometric quantum computation with parametrically tunable coupling," *Phys. Rev. Applied* **10**, 054051 (2018).

[44] Tao Chen and Zheng-Yuan Xue, "High-fidelity and robust geometric quantum gates that outperform dynamical ones," *Phys. Rev. Applied* **14**, 064009 (2020).

[45] Cheng-Yun Ding, Yan Liang, Kai-Zhi Yu, and Zheng-Yuan Xue, "Nonadiabatic geometric quantum computation with shortened path on superconducting circuits," *Applied Physics Letters* **119**, 184001 (2021).

[46] Sai Li, Jing Xue, Tao Chen, and Zheng-Yuan Xue, "High-fidelity geometric quantum gates with short paths on superconducting circuits," *Advanced Quantum Technologies* **4**, 2000140 (2021).

[47] Bao-Jie Liu, Shi-Lei Su, and Man-Hong Yung, "Nonadiabatic noncyclic geometric quantum computation in rydberg atoms," *Phys. Rev. Research* **2**, 043130 (2020).

[48] Yi-Hao Kang, Ye-Hong Chen, Xin Wang, Jie Song, Yan Xia, Adam Miranowicz, Shi-Biao Zheng, and Franco Nori, "Nonadiabatic geometric quantum computation with cat-state qubits via invariant-based reverse engineering," *Phys. Rev. Research* **4**, 013233 (2022).

[49] K. Z. Li, P. Z. Zhao, and D. M. Tong, "Approach to realizing nonadiabatic geometric gates with prescribed evolution paths," *Phys. Rev. Research* **2**, 023295 (2020).

[50] Wei Li, "Invariant-based inverse engineering for fast nonadiabatic geometric quantum computation," *New Journal of Physics* **23**, 073039 (2021).

[51] Jian Zhou, Sai Li, Guo-Zhu Pan, Gang Zhang, Tao Chen, and Zheng-Yuan Xue, "Nonadiabatic geometric quantum gates that are insensitive to qubit-frequency drifts," *Phys. Rev. A* **103**, 032609 (2021).

[52] Bao-Jie Liu, Xue-Ke Song, Zheng-Yuan Xue, Xin Wang, and Man-Hong Yung, "Plug-and-play approach to nonadiabatic geometric quantum gates," *Phys. Rev. Lett.* **123**, 100501 (2019).

[53] K. Z. Li, G. F. Xu, and D. M. Tong, "Coherence-protected nonadiabatic geometric quantum computation," *Phys. Rev. Research* **3**, 023104 (2021).

[54] Bao-Jie Liu, Yuan-Sheng Wang, and Man-Hong Yung, "Super-robust nonadiabatic geometric quantum control," *Phys. Rev. Research* **3**, L032066 (2021).

[55] Yanxiong Du, Zhentao Liang, Hui Yan, and Shiliang Zhu, "Geometric quantum computation with shortcuts to adiabaticity," *Advanced Quantum Technologies* **2**, 1900013 (2019).

[56] Fu-Qiang Guo, Xiao-Yu Zhu, Lei-Lei Yan, Mang Feng, and Shi-Lei Su, "Distinguishment of greenberger-horne-zeilinger states in rydberg atoms via non-cyclic geometric quantum computation," *Annalen der Physik* **533**, 2100057 (2021).

[57] Jian-jian Cheng and Lin Zhang, "Implementing conventional and unconventional nonadiabatic geometric quantum gates via su(2) transformations," *Phys. Rev. A* **103**, 032616 (2021).

[58] Y. Xu, Z. Hua, Tao Chen, X. Pan, X. Li, J. Han, W. Cai, Y. Ma, H. Wang, Y. P. Song, Zheng-Yuan Xue, and L. Sun, "Experimental implementation of universal nonadiabatic geometric quantum gates in a superconducting circuit," *Phys. Rev. Lett.* **124**, 230503 (2020).

[59] Tongxing Yan, Bao-Jie Liu, Kai Xu, Chao Song, Song Liu, Zhensheng Zhang, Hui Deng, Zhiguang Yan, Hao Rong, Kediang Huang, Man-Hong Yung, Yuanzhen Chen, and Dapeng Yu, "Experimental realization of nonadiabatic shortcut to non-abelian geometric gates," *Phys. Rev. Lett.* **122**, 080501 (2019).

[60] J. W. Zhang, L.-L. Yan, J. C. Li, G. Y. Ding, J. T. Bu, L. Chen, S.-L. Su, F. Zhou, and M. Feng, "Single-atom verification of the noise-resilient and fast characteristics of universal nonadiabatic noncyclic geometric quantum

gates,” *Phys. Rev. Lett.* **127**, 030502 (2021).

[61] Ming-Zhong Ai, Sai Li, Zhibo Hou, Ran He, Zhong-Hua Qian, Zheng-Yuan Xue, Jin-Ming Cui, Yun-Feng Huang, Chuan-Feng Li, and Guang-Can Guo, “Experimental realization of nonadiabatic holonomic single-qubit quantum gates with optimal control in a trapped ion,” *Phys. Rev. Applied* **14**, 054062 (2020).

[62] Yang Dong, Shao-Chun Zhang, Yu Zheng, Hao-Bin Lin, Long-Kun Shan, Xiang-Dong Chen, Wei Zhu, Guan-Zhong Wang, Guang-Can Guo, and Fang-Wen Sun, “Experimental implementation of universal holonomic quantum computation on solid-state spins with optimal control,” *Phys. Rev. Applied* **16**, 024060 (2021).

[63] Y.-Y. Huang, Y.-K. Wu, F. Wang, P.-Y. Hou, W.-B. Wang, W.-G. Zhang, W.-Q. Lian, Y.-Q. Liu, H.-Y. Wang, H.-Y. Zhang, L. He, X.-Y. Chang, Y. Xu, and L.-M. Duan, “Experimental realization of robust geometric quantum gates with solid-state spins,” *Phys. Rev. Lett.* **122**, 010503 (2019).

[64] D. A. Lidar, I. L. Chuang, and K. B. Whaley, “Decoherence-free subspaces for quantum computation,” *Phys. Rev. Lett.* **81**, 2594–2597 (1998).

[65] L.-A. Wu, P. Zanardi, and D. A. Lidar, “Holonomic quantum computation in decoherence-free subspaces,” *Phys. Rev. Lett.* **95**, 130501 (2005).

[66] Almut Beige, Daniel Braun, Ben Tregenna, and Peter L. Knight, “Quantum computing using dissipation to remain in a decoherence-free subspace,” *Phys. Rev. Lett.* **85**, 1762–1765 (2000).

[67] Paul G. Kwiat, Andrew J. Berglund, Joseph B. Altepeter, and Andrew G. White, “Experimental verification of decoherence-free subspaces,” *Science* **290**, 498–501 (2000).

[68] Daniel A. Lidar and K. Birgitta Whaley, “Decoherence-free subspaces and subsystems,” in *Irreversible Quantum Dynamics*, edited by Fabio Benatti and Roberto Floreanini (Springer Berlin Heidelberg, Berlin, Heidelberg, 2003) pp. 83–120.

[69] D. Bacon, J. Kempe, D. A. Lidar, and K. B. Whaley, “Universal fault-tolerant quantum computation on decoherence-free subspaces,” *Phys. Rev. Lett.* **85**, 1758–1761 (2000).

[70] Peng Xue and Yun-Feng Xiao, “Universal quantum computation in decoherence-free subspace with neutral atoms,” *Phys. Rev. Lett.* **97**, 140501 (2006).

[71] Man-Duen Choi and David W. Kribs, “Method to find quantum noiseless subsystems,” *Phys. Rev. Lett.* **96**, 050501 (2006).

[72] Lorenza Viola, Evan M. Fortunato, Marco A. Pravia, Emanuel Knill, Raymond Laflamme, and David G. Cory, “Experimental realization of noiseless subsystems for quantum information processing,” *Science* **293**, 2059–2063 (2001).

[73] J. Zhang, L.-C. Kwek, Erik Sjöqvist, D. M. Tong, and P. Zanardi, “Quantum computation in noiseless subsystems with fast non-abelian holonomies,” *Phys. Rev. A* **89**, 042302 (2014).

[74] Evan M. Fortunato, Lorenza Viola, Marco A. Pravia, Emanuel Knill, Raymond Laflamme, Timothy F. Havel, and David G. Cory, “Exploring noiseless subsystems via nuclear magnetic resonance,” *Phys. Rev. A* **67**, 062303 (2003).

[75] Daniel A. Lidar, “Review of decoherence-free subspaces, noiseless subsystems, and dynamical decoupling,” in *Quantum Information and Computation for Chemistry* (John Wiley & Sons, Ltd, 2014) pp. 295–354.

[76] Lorenza Viola, Emanuel Knill, and Seth Lloyd, “Dynamical decoupling of open quantum systems,” *Phys. Rev. Lett.* **82**, 2417–2421 (1999).

[77] Alexandre M. Souza, Gonzalo A. Álvarez, and Dieter Suter, “Robust dynamical decoupling,” *Philosophical Transactions of the Royal Society A: Mathematical, Physical and Engineering Sciences* **370**, 4748–4769 (2012).

[78] K. Khodjasteh and D. A. Lidar, “Fault-tolerant quantum dynamical decoupling,” *Phys. Rev. Lett.* **95**, 180501 (2005).

[79] Michael J. Biercuk, Hermann Uys, Aaron P. VanDevender, Nobuyasu Shiga, Wayne M. Itano, and John J. Bollinger, “Optimized dynamical decoupling in a model quantum memory,” *Nature* **458**, 996–1000 (2009).

[80] E. L. Hahn, “Spin echoes,” *Phys. Rev.* **80**, 580–594 (1950).

[81] Guofu Xu and Guilu Long, “Protecting geometric gates by dynamical decoupling,” *Phys. Rev. A* **90**, 022323 (2014).

[82] P. Z. Zhao, X. Wu, and D. M. Tong, “Dynamical-decoupling-protected nonadiabatic holonomic quantum computation,” *Phys. Rev. A* **103**, 012205 (2021).

[83] X. Wu and P. Z. Zhao, “Nonadiabatic geometric quantum computation protected by dynamical decoupling via the xxz hamiltonian,” *Frontiers of Physics* **17**, 31502 (2021).

[84] X. Wu and P. Z. Zhao, “Universal nonadiabatic geometric gates protected by dynamical decoupling,” *Phys. Rev. A* **102**, 032627 (2020).

[85] Xing-Long Zhen, Fei-Hao Zhang, Guanru Feng, Hang Li, and Gui-Lu Long, “Optimal experimental dynamical decoupling of both longitudinal and transverse relaxations,” *Phys. Rev. A* **93**, 022304 (2016).

[86] F. F. Fanchini, R. d. J. Napolitano, B. Çakmak, and A. O. Caldeira, “Protecting the $\sqrt{\text{swap}}$ operation from general and residual errors by continuous dynamical decoupling,” *Phys. Rev. A* **91**, 042325 (2015).

[87] Alexandre M. Souza, Gonzalo A. Álvarez, and Dieter Suter, “Experimental protection of quantum gates against decoherence and control errors,” *Phys. Rev. A* **86**, 050301 (2012).

[88] Lorenza Viola, Seth Lloyd, and Emanuel Knill, “Universal control of decoupled quantum systems,” *Phys. Rev. Lett.* **83**, 4888–4891 (1999).

[89] K. V. Kepesidis, M.-A. Lemonde, A. Norambuena, J. R. Maze, and P. Rabl, “Cooling phonons with phonons: Acoustic reservoir engineering with silicon-vacancy centers in diamond,” *Phys. Rev. B* **94**, 214115 (2016).

[90] D F James and J Jerke, “Effective hamiltonian theory and its applications in quantum information,” *Canadian Journal of Physics* **85**, 625–632 (2007).

[91] E Brion, L H Pedersen, and K Mølmer, “Adiabatic elimination in a lambda system,” *Journal of Physics A: Mathematical and Theoretical* **40**, 1033 (2007).

[92] Ph. Tamarat, T. Gaebel, J. R. Rabeau, M. Khan, A. D. Greentree, H. Wilson, L. C. L. Hollenberg, S. Prawer, P. Hemmer, F. Jelezko, and J. Wrachtrup, “Stark shift control of single optical centers in diamond,” *Phys. Rev. Lett.* **97**, 083002 (2006).

[93] V. M. Acosta, C. Santori, A. Faraon, Z. Huang, K.-M. C. Fu, A. Stacey, D. A. Simpson, K. Ganesan,

S. Tomljenovic-Hanic, A. D. Greentree, S. Prawer, and R. G. Beausoleil, “Dynamic stabilization of the optical resonances of single nitrogen-vacancy centers in diamond,” *Phys. Rev. Lett.* **108**, 206401 (2012).

[94] Bruce W. Shore and Peter L. Knight, “The jaynes-cummings model,” *Journal of Modern Optics* **40**, 1195–1238 (1993).

[95] Michael J. Bremner, Christopher M. Dawson, Jennifer L. Dodd, Alexei Gilchrist, Aram W. Harrow, Duncan Mortimer, Michael A. Nielsen, and Tobias J. Osborne, “Practical scheme for quantum computation with any two-qubit entangling gate,” *Phys. Rev. Lett.* **89**, 247902 (2002).

[96] Jacob R. West, Daniel A. Lidar, Bryan H. Fong, and Mark F. Gyure, “High fidelity quantum gates via dynamical decoupling,” *Phys. Rev. Lett.* **105**, 230503 (2010).